Available online at www.ijournalse.org

Emerging Science Journal

(ISSN: 2610-9182)

Vol. 10, No. 1, February, 2026

Performance Evaluation of Inclined-Step and Wall Roughness on Battery Thermal Management System

Olanrewaju M. Oyewola [1*], Emmanuel T. Idowu [1], Morakinyo J. Labiran [1], Michael C. Hatfield [2], Mebougna L. Drabo [3]

[1] *Department of Mechanical Engineering, University of Alaska Fairbanks, Fairbanks, AK 99775, United States.*

[2] *Department of Electrical and Computer Engineering, University of Alaska Fairbanks, Fairbanks, AK 99775, United States.*

[3] *Department of Mechanical & Civil Engineering and Construction Management, Alabama A&M University, Huntsville, AL 35811, United States.*

Abstract

In this study, the effects of inclined steps and wall roughness on the step-like plenum of the Z-type battery thermal management system (BTMS) are examined, extending the literature on its design. Due to the performance of the design in achieving a reduction in maximum temperature (T_{max}), additional modifications are required to provide more insight into further enhancing the thermal performance and overcoming the design's drawback, such as higher pressure drop (ΔP). The performance of the system was evaluated in terms of the T_{max} and maximum temperature difference (ΔT_{max}) of batteries in the systems and ΔP across the system. The temperature values were selected after comparing the maximum temperatures recorded on each battery. Investigations were carried out using a Computational Fluid Dynamics (CFD) method, which was validated by comparing with experimental data from the literature. Findings revealed that the step designs with inclined angles of 5°, 45° and 85° reduced the T_{max} by 3.18 K, 3.9 K, and 4.34 K, respectively, when compared to the Z-type design. However, the Z-type design has the lowest ΔP value (16.50 Pa), while the original step-like design system produced the highest value (20.96 Pa). When considering the roughness, by increasing the roughness height from 5 μm to 10 μm, an increase in T_{max} was observed, while wall roughness generally decreases the ΔP. From 0 to 10 μm, T_{max} increased by 0.03 K (0.01 %) and ΔP increased by 0.07 Pa (0.29 %), indicating negligible effects. The study, therefore, concludes that adequate selection of step design with different angles, air inlet velocity, temperature, and wall roughness will be highly beneficial for designing cost-effective and efficient BTMSs.

Keywords:

Inclined-Step;
Wall Roughness;
Divergence Plenum;
Velocity;
Temperature;
Pressure Drop;
Thermal Management Systems.

Article History:

Received:	12	July	2025
Revised:	24	January	2026
Accepted:	28	January	2026
Published:	01	February	2026

1- Introduction

The use of batteries as a clean energy source in the transport industry to power electric vehicles (EVs) has gained significant popularity. Babu Sanker & Baby [1] reported that the use of electric vehicles can decrease the emission of substances that deplete the ozone layer by about 40%. The most common type of rechargeable battery available in the electrical energy storage market is the Lithium-ion battery [2]. Lithium batteries are highly sensitive to temperature, and hence their working temperature must be maintained between 15 ℃ to 45 ℃, while the maximum temperature difference in the case of multiple batteries working together must be less than 5 ℃ [3-5]. Operating in a hot environment or under prolonged, severe driving conditions will shorten battery life and cause uneven temperature variation among batteries. It is therefore imperative to develop a system that offsets excess heat generated by the batteries while maintaining their temperature within an acceptable range during charging and discharging. Such a system is generally referred to as a Battery Thermal Management System (BTMS). Over the years, different BTMS have been developed and categorized according to the cooling mode as active or passive. For active-cooling, heat is dissipated through the direct contact of

* **CONTACT**: ooyewola@alaska.edu; oooyewola001@gmail.com

DOI: http://dx.doi.org/10.28991/ESJ-2026-010-01-01

cooling fluid; air [6-10], heat pipe [11, 12], or liquid [13, 14]. In passive cooling, heat is removed using a phase change material (PCM) [15-17]. With continuous advances in research, a combination of two or more cooling methods, whether passive/passive, passive/active, or active/active, has been adopted, and such systems are generally referred to as hybrid BTMS [18-21]. The hybrid BTMS leverages the benefits of different cooling methods to develop more efficient BTMS. Typically, each of these systems has unique advantages; however, the air-cooling BTMS remains the preferred method for EVs due to its low cost, long service life, and good expandability. Despite these advantages, air cooling remains susceptible to high temperature differences within the battery pack in the BTMS, due to air's low heat capacity [9, 10]. Hence, extensive research has been conducted and is ongoing on air-cooled BTMS to improve the system's temperature uniformity.

The parallel air-cooled Z-type design is widely investigated with studies changing air flow pattern [9, 24], adjusting the spacing between batteries [22-25], installing spoilers, plate, fins or baffles along the air flow path [8-10, 26, 27], changing the angle of inclination of the inlet and outlet channels [28], reducing the size (inclined, curved or step-like) of DP and/or CP [29-34]. Chen et al. [32] optimized Z-type and U-type BTMS by adjusting plenum width and using the CFD method and flow resistance network model. Results showed a 70% reduction in temperature difference among batteries and a 32% reduction in power consumption when the inlet and outlet widths were optimized. Chen et al. [34] optimized the Z-type air-cooled BTMS structure by adjusting the plenum width to reduce the air velocity standard deviation, thereby lowering the maximum temperature by 1.2 K for a fixed inlet flow rate. In a study by Yu et al. [35], vertical spoilers were installed to improve cooling performance, resulting to a 9.2℃ reduction in the maximum temperature and a 5℃reduction in the maximum temperature difference. Wang et al. [27] extended the work by varying the number, length, cooling channel spacing, width, and angle of inclination of spoilers installed along cooling channels. The optimized design reduced the maximum temperature by 3.52 K when compared to the BTMS without spoilers.

Furthermore, Zhang et al. [8] investigated the effects of the spoiler's vertical height after it was inclined to an angle, in addition to the position and quantity of spoilers. By considering optimized parameters and installing a spoiler in the first cooling channel, the maximum temperature and maximum temperature difference were reduced by 3.39 K and 5.87 K, respectively. Wang et al. [36] optimized the Z-type BTMS by adding parallel plates to alter air flow distribution. An optimization scheme with four parallel plates improved the BTMS's performance by 3.37 K and 5.5 K compared to the original Z-type BTMS. Wang et al. [9] studied the impact of parallel plates on Z-type BTMS and identified eight unique flow patterns. Four design optimization schemes were adopted for flow pattern designs. The optimized designs with parallel plates reduced the maximum temperature and temperature difference by 3.42 K and 6.4 K, respectively, compared to the original Z-type BTMS. Oyewola et al. [33] adopted a step-like design for the divergence plenum of the BTMS. A 7-step case model yielded the best system's maximum temperature of 324.9 K and cell temperature difference of 1 K, both 3.94 K and 5.93 K, respectively, lower than that of the Z-type BTMS. Similar to the approach adopted by Wang et al. [9], the step-like design, initially investigated only for the Z-type flow pattern, was further studied by Oyewola & Idowu [37]. The results showed improvement, reducing the maximum temperature and maximum temperature difference by 3.24 K and 7.62 K, respectively, compared to an original design with a specific flow pattern without steps.

Other researchers focused on the effect of the cooling fluid or medium temperature on BTMS performance [38, 39, 40]. In the study by Li et al. [38], the adaptability of lithium-ion battery-powered unmanned aerial vehicles (UAVs) under severe environmental temperature conditions was investigated. It was reported that at a temperature of about 60℃, a significant effect on the UAV's flying performance. At a temperature of about -25℃, the flying performance and battery performance of the UAV were decreased considerably. Wei et al. [39] investigated a liquid-cooled battery thermal management system, focusing on the effects of liquid-cooling plate connections, coolant inlet temperature, and ambient temperature on the system's thermal performance. The proposed cooling strategy reduced the maximum temperature difference in the system by about 36% at the start of discharge. Verma & Saraswati [40] compared air-cooled lithium-ion battery packs with staggered and aligned arrangements. They found that the staggered arrangement reduced battery temperature and provided better temperature uniformity compared to the aligned arrangement. Studies have also leveraged the benefits of machine learning (ML) tools to optimize the performance of BTMSs by reducing the number of repeated experiments and trials [41 - 43]. Tran et al. [41] developed prediction models for high-capacity lithium-ion battery thermal and electrical performance using Python-based scikit-learn ML. Four machine learning models (k-nearest neighbors, linear regression, random forests, and decision trees) were tested and validated with experimental data. The decision tree-based model was the best, with an R^2 value of 0.99.

A study by Billert et al. [42], examined the potential of predictive BTMS by adopting Quantile Convolutional Neural Networks (QCNN), which provides battery temperature predictions based on given input data. By adopting the QCCN, predictions were made, and BTMS energy efficiency was increased while accounting for ageing and de-rating effects. Khaboshan et al. [43] conducted a parametric investigation of a battery thermal management system with phase change material, fins, and metal foam using CFD and ANN approaches. They found that integrating passive cooling approaches maintains the lowest temperature, with the optimum BTMS reducing by 3 K compared to pure PCM. Several designs have also emerged in recent years, covering cooling strategies such as air cooling (AC) [44, 45], phase change material cooling (PCMC) [46, 47], heat pipe cooling (HPC) [48], liquid cooling (LC) [49, 50], hybrid cooling (HC) [51, 52]. Focusing on the potential of the air-cooling technique, Oyewola & Idowu [44] investigated the effects of different configurations of straight and wave-like plenums. The study focused on maximum recorded battery temperatures and using a wave-inclined plenum design, T_{max}, and ΔT_{max} were reduced by 4.61 K and 8 K, respectively, when compared

with the Z-type BTMS. In the work of Wu et al. [46], based on Fin-PCM in variable gravitational acceleration (GA). The study suggests that adjusting the angle of inclination (θ) can improve PCM performance in BTMS. Wu et al. [49] proposed a novel cooling plate design for liquid-cooled BTMS with a variable heat transfer path (VHTP). The optimized cooling plate reduces the temperature difference across the battery surface from 22.7% to 25.4%, while slightly increasing the maximum battery surface temperature. Dilbaz et al. [51] conducted a comparative study of phase change material cooling (PCMC), nano-enhanced channel cooling (NECC), and hybrid cooling (HC) methods. The study found that the HC method reduced maximum temperature by 28%, while PCMC and NECC reduced it by 26% and 27%, respectively.

From the reviewed studies, the maximum temperature reduction has been achieved; however, it remains insufficient, especially when the ambient temperature is extremely hot or cold. Additionally, some designs will add weight to the system and can create undesired vibration at higher air velocities. For instance, designs with spoilers can introduce additional material and vibration, and liquid and PCM cooling will add weight compared to air cooling. Hence, air-cooling design remains a favourite technique, and among the reported studies, the step-like design by Oyewola et al. [33] presents a valuable outcome and has been further investigated to gain more insight into its performance with different additional structural modifications. Research has also shown that surface roughness can influence fluid dynamics and heat transfer [53-55]. According to Kadivar et al. [55], a detailed investigation of the reported influence of surface roughness can either negatively or positively affect system performance. The study further noted that despite significant progress, the structure of turbulent flow remains poorly understood. An extensive study of turbulent flow in different applications involving heat transfer and fluid flow is critical, especially in the field of battery thermal management systems, which, to the best of the authors' knowledge, has not been reported in the literature. This study, therefore, extends the work of Oyewola et al. [33] to further explore several additional considerations for the design. Firstly, the cooling air is of ambient temperature, which varies by region and season; hence, the effect of variation in cooling air temperature was investigated. Secondly, studies investigated the performance of smooth surfaces; however, in reality, the surfaces of heat transfer equipment exhibit varying degrees of wall roughness, which can be intentionally introduced through advanced additive manufacturing or unintentionally through manufacturing defects (e.g., machining) and operational factors (e.g., fouling). Therefore, this study also considered the influence of wall roughness on the performance of the systems using the default setting in Ansys Fluent, without introducing physical roughness. Lastly, the enhanced thermal performance of the original step-like comes at the cost of increased pressure drop, and several studies have sought to reduce it. This study also explored a step-inclination concept to reduce pressure drop. A generalized summary of the article consists of the abstract, introduction, methodology, results and discussions, conclusions, declaration, and references.

2- Research Methodology

2-1- Z-Type Physical Model

The Z-type model was selected for this study based on its widespread use among researchers and the availability of experimental results in the literature. Figure 1 (a) and (b) show 2D geometries of the BTMS model and a battery, respectively, while Figure 2 shows the 3D geometry of the Z-type model. In the study by Chen et al. [23], the performance of the Z-type model was investigated experimentally. The Z-type model consists of inlet and outlet sections through which cooling air enters and leaves, respectively, after cooling down the eight batteries in the system. During battery cooling, the cooling air also passes through nine cooling channels (CCs). The length of each cooling channel (CC_l) is fixed at 3 mm, temperature and velocity of cooling air enters the system at 3 m/s and 298.15 K, respectively, while the heat power of each battery was 11.8W. The rate of battery heat generation was adopted from a study by Chen et al. [24], where the rate of heat generation for 5-C constant-discharge cycles of a 12Ah LiFePO4 battery was estimated to be 69370 W/m^3, corresponding to a heat power of 11.8W per battery. The thermophysical properties of air and the battery are shown in Table 1. The Z-type model, including its geometric configuration and dimensions, is shown in Table 2. This study also considered a 2D model for all numerical simulations. This is based on the recommendations from the study of Chen et al. [23], which suggests that using a 3D model takes longer than a 2D model. The study further established that numerical simulations in both 2D and 3D yielded nearly identical results, with average relative errors of 1% and 0.1% for air flow rate and battery temperature, respectively.

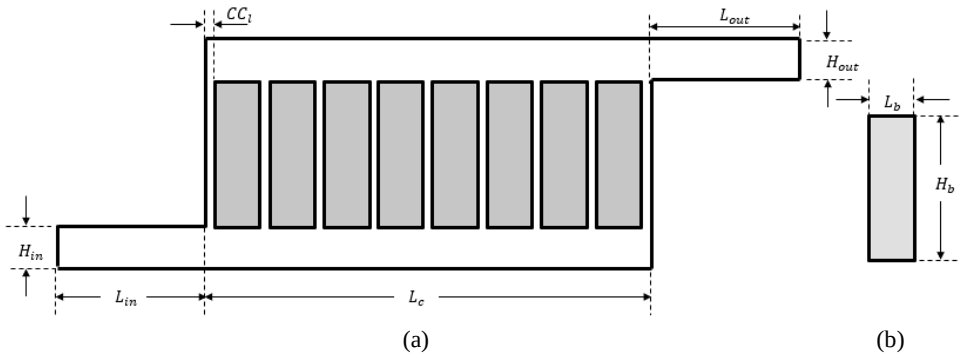

Figure 1. (a) 2D geometry of Z-Type BTMS, and (b) 2D geometry of a battery

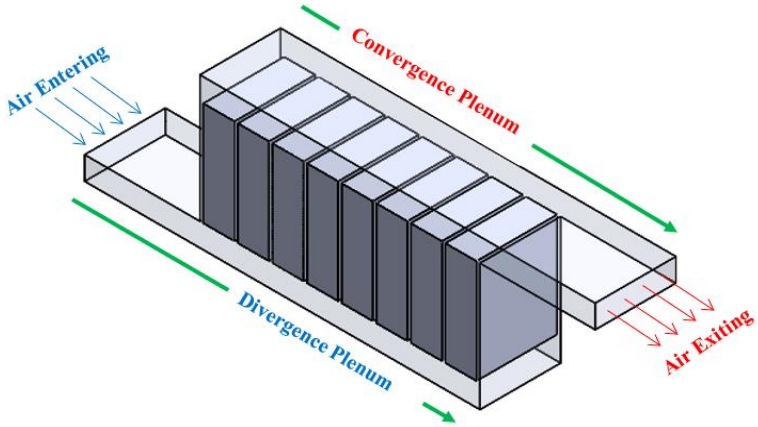

Figure 2. 3D geometry of Z-Type BTMS

Table 1. Thermo-physical properties of battery and air [23, 33]

Property	Unit	Battery	Air
Dynamics viscosity	kg/ms	-	1.86×10^{-5}
Specific heat	J/kgK	1337	1005
Density	kg/m^3	1542.9	1.165
Thermal conductivity	W/mK	x = 1.05; y = 21.1	0.0267

Table 2. Geometrical parameters of the Z-type [23, 33]

Description	Symbol	Value (mm)
Cooling channel length	CC_l	3
Manifold inlet/outlet length	L_{in}/L_{out}	100
Cooling section length	L_c	243
Battery length	L_b	27
Manifold inlet/outlet length	H_{in}/H_{out}	20
Battery height	H_b	90
Manifold inlet/outlet width	W_{in}/W_{out}	70
Battery width	W_b	70
Convergence/Divergence plenum	C_p/D_p	343

2-2- Step-like Physical Models

The step-like model, proposed by Oyewola et al. [33], is a modification of the Z-type BTMS, with the divergence plenum redesigned. The step parameters include a step length L_s, step height H_s, and number of steps N_s. Figures 3 (a) and (b) show a 2D schematic view and a 3D isometric view of the step-like BTMS. In this design, the divergence plenum was designed based on equal step height. The height of steps and length of steps are estimated using Equations 1 and 2, respectively. Additional information and description on the design of the steps in the step-like BTMS can be found in the work of Oyewola et al. [33]. To further investigate the temperature and air flow distribution of the step-like BTMS, the inclination of the step height was considered. In the new proposed modification, the height (vertical) was maintained as the normal step height presented in Figure 3 (a) and Table 3, while the initial position of the step height was inclined at an angle, while also maintaining the height (vertical) as illustrated in Figure 4 (a). Figure 4 (b) further shows a 3D isometric view of the step-like model with inclined steps at an angle θ.

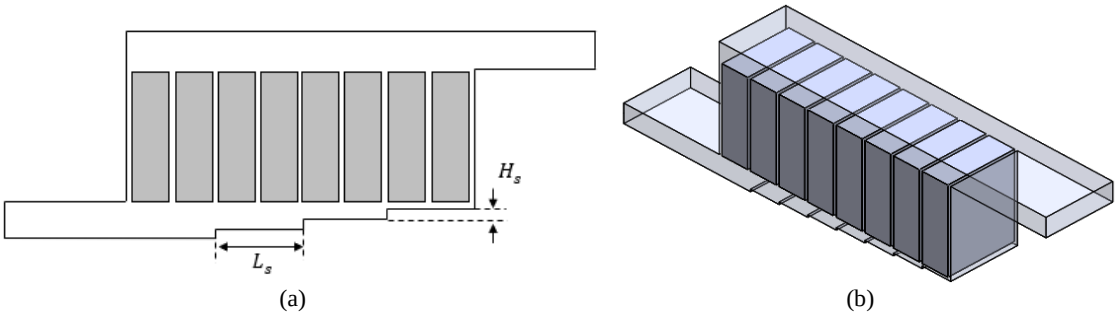

(a) (b)

Figure 3. Step-like BTMS (a) 2D Schematic view (b) 3D Isometric view

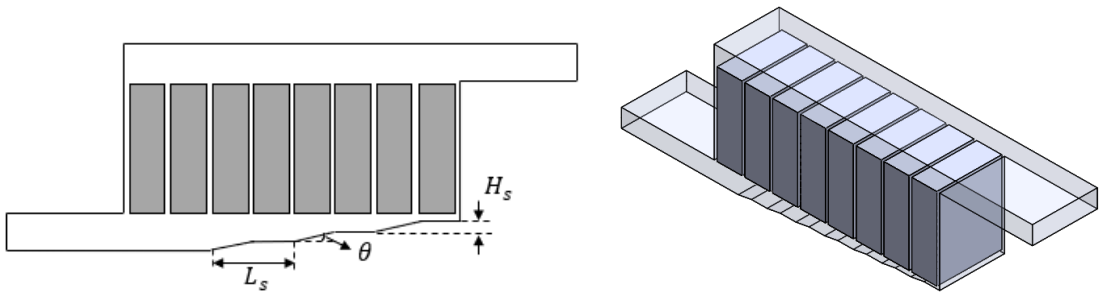

(a) (b)

Figure 4. Inclined-step BTMS (a) 2D Schematic view (b) 3D Isometric view

$$H_s = \frac{H_{in}}{N_s+1} \quad (1)$$

$$L_s = \frac{L_c - CC_l}{N_s+1} \quad (2)$$

Table 3. Geometrical and operational parameters of the inclined-step BTMSs

Description	Symbol	Value	Unit
Length of step	L_s	30	mm
Number of steps	N_s	7	-
Height of step	H_s	2.5	mm
Air inlet velocity	v	3, 5, 7	m/s
Air inlet temperature	T_{in}	278, 298, 318	K
Inclined angle of step	θ	5, 45, 85	°
Roughness height	K_s	5, 10	μm

2-3- Numerical Solution

2-3-1- Data Reduction

The air and temperature distribution performance of the BTMS was analyzed using the ANSYS Fluent CFD platform. The performance of the systems was determined by comparing parameters obtained from BTMS after numerical solutions were complete, and the results were extracted. Parameters such as the maximum battery temperature (T_{max}), maximum battery temperature difference (ΔT_{max}) of the batteries, and pressure drop (ΔP) for each system were the primary focus of investigation. ΔT_{max} is the difference between the maximum temperature (T_{max}) and the minimum temperature (T_{min}) of the eight batteries. Equation 3 and 4 gives the mathematical representation for ΔT_{max} and ΔP, respectively.

$$\Delta T_{max} = T_{max} - T_{min} \quad (3)$$

$$\Delta P = P_{in} - P_{out} \quad (4)$$

where: P_{in} and P_{out} are the maximum pressures of air at the inlet and outlet sections of BTMS, respectively, A is the cross-sectional area at the inlet, and v is the air velocity at the inlet of the BTMS.

In numerical simulation, determining whether the flow is laminar or turbulent is crucial, which is achieved by estimating the Reynolds number at the inlet section of the system. The BTMS can be modelled as either a 3D or a 2D geometry, as established in the literature [23], yielding very similar performance with negligible differences. Reynolds number, Re (5) at minimum air inlet velocity ($v = 3\,m/s$) was estimated to be 5825, hence a turbulent flow was considered. Since available experimental studies are only for 3D geometries, the hydraulic diameter estimated in this study is based on the 3D air inlet cross-section, given by Equation 6;

$$Re = \frac{\rho v D_h}{\mu} \quad (5)$$

$$D_h = \frac{2W_{in}H_{in}}{W_{in}+H_{in}} \quad (6)$$

where: W_{in} is the width of inlet manifold, H_{in} is the height of the inlet manifold, ρ is density of cooling air (kg/m^3), v is cooling air inlet velocity (m/s), μ is dynamic viscosity (kg/ms) of air and D_h is hydraulic diameter of inlet section (m).

2-3-2- Numerical Model

To accurately model the physics of turbulence near a wall, wall functions are utilized to bridge the logarithmic-layer and wall-layer of the turbulence boundary layer, consequently allowing for a coarser mesh near the wall and minimizing

the computational demands [53]. When considering rough walls, surface roughness parameters are assigned, which modify the wall functions using the equivalent sand-grain roughness approach. However, this cannot be assigned when enhanced wall function is selected. The initial selection of enhanced wall treatment was based on the general recommendation from the literature and its accuracy to model near wall effects without the need to introduce wall roughness characteristics. However, in reality, surfaces are rarely perfectly smooth, hence, for investigations requiring wall roughness, standard wall treatment was selected which has the options to specify and/or modify wall roughness characteristics.

The flow of air into the system is in a steady state, having a uniform velocity distribution. The following assumptions were also made:

- Flow is incompressible, while air density is taken as constant,
- Fluid is isotropic and Newtonian and;
- Gravitational effect, radiation, and chemical reaction were considered to be negligible.

Flow governing equations were considered, such as the continuity Equation 7 and the momentum Equation 8, to compute time-dependent flow. At the same time, the energy Equation 9 was also adopted for time-dependent thermal solution [27, 33, 38].

$$\nabla \cdot \overrightarrow{v} = 0 \tag{7}$$

$$\rho \frac{\overrightarrow{dv}}{dt} = -\nabla p + \mu \nabla^2 \overrightarrow{v} \tag{8}$$

$$\rho c \frac{\partial T}{\partial t} + \nabla \cdot (\rho c \overrightarrow{v}\, \mathrm{T}) = \nabla \cdot (k \nabla T) \tag{9}$$

Since the flow is turbulent as earlier determined, the standard k-e turbulence model 10 and 11, with enhanced wall treatment was selected for the solution [27, 33, 38].

Equation for turbulence kinetic energy, k;

$$\frac{\partial}{\partial t}(\rho k) + \frac{\partial}{\partial x_i}(\rho k u_i) = \frac{\partial}{\partial x_j}\left[\left(\mu + \frac{\mu_t}{\sigma_k}\right)\frac{\partial k}{\partial x_j}\right] + G_k + G_b - \rho\varepsilon - Y_M + S_k \tag{10}$$

Equation for turbulent energy dissipation, ε;

$$\frac{\partial}{\partial t}(\rho \varepsilon) + \frac{\partial}{\partial x_i}(\rho \varepsilon u_i) = \frac{\partial}{\partial x_j}\left[\left(\mu + \frac{\mu_t}{\sigma_\varepsilon}\right)\frac{\partial \varepsilon}{\partial x_j}\right] + C_{1\varepsilon}\frac{\varepsilon}{k}(G_k + C_{3\varepsilon}G_b) - C_{2\varepsilon}\rho\frac{\varepsilon^2}{k} + S_\epsilon \tag{11}$$

Turbulent viscosity is given as;

$$\mu_t = \rho C_\mu \frac{k^2}{\varepsilon} \tag{12}$$

Equations 10 to 12 model constants are $C_{1\varepsilon} = 1.44,\ C_{2\varepsilon} = 1.92,\ C_\mu = 0.09$, $\sigma_k = 1.0$ and $\sigma_\epsilon = 1.3$.

A shift in the logarithmic velocity profile Equation 13 will occur due to the impact of wall roughness.

$$u_\tau = \frac{|u|}{\frac{1}{k_V}\ln\delta_w^+ + B - \Delta B} \tag{13}$$

where ΔB is a shift factor depending on the non-dimensional roughness height (k_s^+)

For a sand-grain roughness and similar types of uniform roughness elements, ΔB is well-correlated with the non-dimensional roughness height Equation 14;

$$\mathrm{k}_s^+ = \frac{\rho\left(c_\mu^{1/4}\sqrt{k}\right)k_s}{\mu} \tag{14}$$

Here k_s is the step physical roughness height, and ΔB is defined differently for different roughness regimes [54]. In addition to the roughness height, the roughness constant (C_s) must also be assigned.

Energy conservation equation for battery [33, 37] is;

$$\rho_b c_b \frac{\partial T}{\partial t} = \nabla \cdot (k_b \nabla T) + Q \tag{15}$$

Furthermore, the SIMPLE algorithm was selected to solve the pressure-based governing equations, while the discretization of diffusive and convective terms was achieved using second-order and central-differencing terms [36-38]. Finally, the iteration residuals for convergence criteria were set at 10^{-8} and 10^{-6} for the energy and flow terms, respectively.

2-3-3- Boundary Conditions

For the initial simulations to achieved validation of the numerical procedure, air inlet velocity condition of 3, 3.5 and 4 m/s were assigned to the inlets of the BTMS, each at temperature of 298.15 K. Afterwards, pressure-outlet condition was assigned to the outlet section, to enable prediction of pressure drop between inlet and outlet sections of the BTMS, assuming surrounding pressure to be atmospheric pressure. Additionally, non-slip conditions were assigned to the internal walls of the batteries and system, while the system's external walls were assigned adiabatic conditions. Wall surface roughness parameters were also assigned for BTMSs with and without steps. The surface is assumed to be roughened with tightly packed, uniform sand-grain roughness. A summary of all the boundary conditions assigned to the BTMSs is presented in Table 4.

The following assumptions were also considered:

- Properties of air and battery are constant,
- Surrounding temperature and pressure remain constant,
- The heat generation rate of the battery is constant.

Table 4. Boundary conditions used after validation of the numerical solution

Part	Boundary condition	Symbol	Value	Unit
Plenum Inlet	Air inlet velocities	v	3, 5, 7	m/s
	Air inlet temperatures	T_{in}	278, 298, 318	K
Plenum Outlet	Pressure outlet	P_{out}	Zero (0)	Pa
Battery wall	No-Slip	-	-	-
System inner wall	No-Slip	-	-	-
Divergence plenum wall roughness	Roughness height	K_s	5, 10	μm
	Roughness constant	C_s	0.5	-
System outer wall	Adiabatic	-	-	-

2-3-4- Meshing and Independence Study

The quality of the mesh generated for each BTMS geometry significantly influences the accuracy of the simulation results, along with boundary conditions and selected computational models. The mesh independence study compares numerical solution results from a specific model at different mesh resolutions. To achieve a mesh-independent solution, a structural mesh with five inflation layers, and a first layer height (y^+) of 0.1 mm at both the system and battery wall was assigned to cater for the boundary layers [33, 38]. T_{min} and ΔT_{max} of the original Z-design were used to evaluate the independence of the meshes. The stability of T_{min} and ΔT_{max} as the number of elements increases is displayed in Figure 5. As the number of elements increased above 410,729, the change in the values of T_{min} and ΔT_{max} stabilizes, with a difference of 0.13 K and 0.42 K, respectively. Therefore, similar mesh settings to those for a mesh size of 410,729 were adopted for the other geometries in this study.

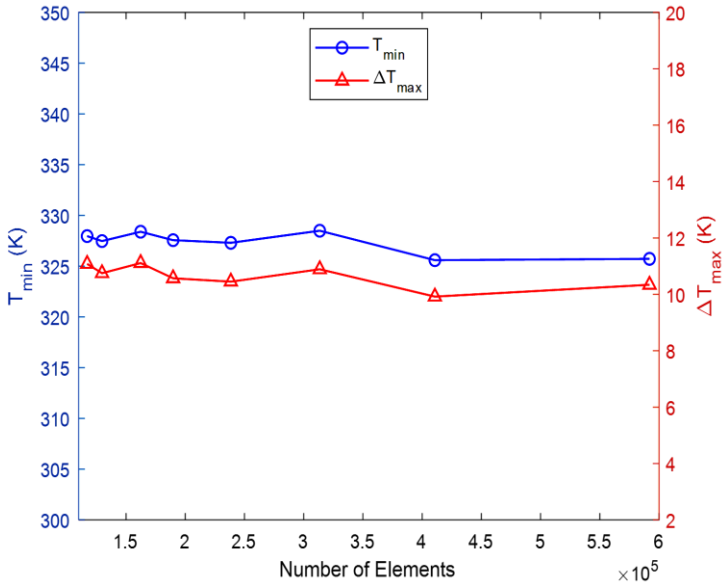

Figure 5. Mesh sensitivity study of Z-design BTMS

2-3-5- Validation of Numerical Solution

Results for the original Z-type BTMS were compared with those from [23]. Temperature of batteries at inlet air velocities of 3, 3.5, and 4 m/s were used for comparison. For the experimental results, thermocouples were placed at the centre of the battery blocks. Afterwards, T_{max} and T_{min} were measured at the second and eighth batteries, respectively. The difference $\Delta T_{max} = T_{max} - T_{min}$ was also estimated, known as the maximum temperature difference. To verify the accuracy of the numerical solution, simulations were performed under conditions similar to those in the experiment. The comparison between simulation and experiment of Chen et al. [23] is displayed in Figure 6 (a) for T_{max} when the enhanced wall treatment and standard wall treatment were employed, respectively. Firstly, the two wall treatments were considered to determine the preferred wall treatment based on deviations from experimental data. Secondly, only the scalable wall treatment allows wall roughness to be modelled. The validation showed that the absolute maximum deviations of 3.31 K (0.6 %) and 4.50 K (1.35%), respectively, were obtained for the enhanced wall treatment and the standard wall treatment. A relative error of approximately 2% is acceptable, as reported by Zhang et al. [8] in a study on the design of air-cooled BTMS.

Furthermore, Alzwayi & Paul [10] reported that increasing the mesh resolution reduces the estimated percentage deviation; however, this will require longer computation time. Hence, a percentage deviation close to 5% is often considered acceptable when using a lower mesh resolution. Moreover, the same mesh settings must be maintained for any other geometry considered. Hence, the simulation procedure adopted in this study is considered acceptable and reliable. It should be noted that the enhanced wall treatment was used for all solutions that do not require wall roughness. In contrast, the standard wall treatment was used for solutions that do require wall roughness. The comparison between the experimental study by Chen et al. [23] and simulation results obtained using the enhanced wall treatment is presented as Figure 6 (b) and (c), for T_{max} and T_{min}, respectively. From the results, maximum deviation of 3.31 K (0.6 %) and 1.49 K (1.2 %) for T_{max} and T_{min}, respectively were estimated. The 2D geometry, selected grid, air temperature, and velocity contours for the original Z-type BTMS are presented as Figures 7 (a) to (d), respectively. A summary of the research methodology is presented using a flowchart as Figure 8.

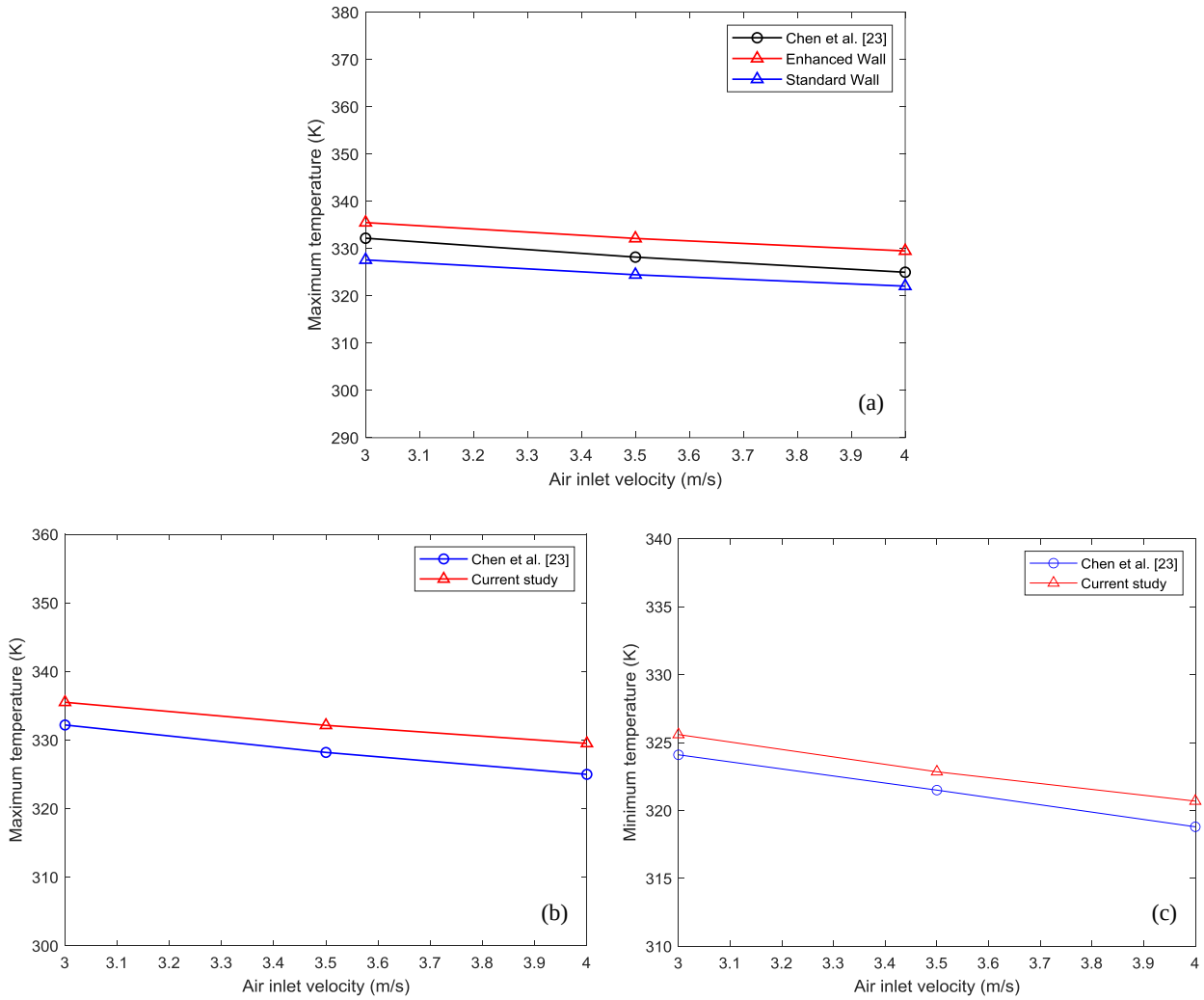

Figure 6. Comparison of (a) T_{max} for two turbulence models, (b) T_{max} and (c) T_{min} for enhanced wall treatment.

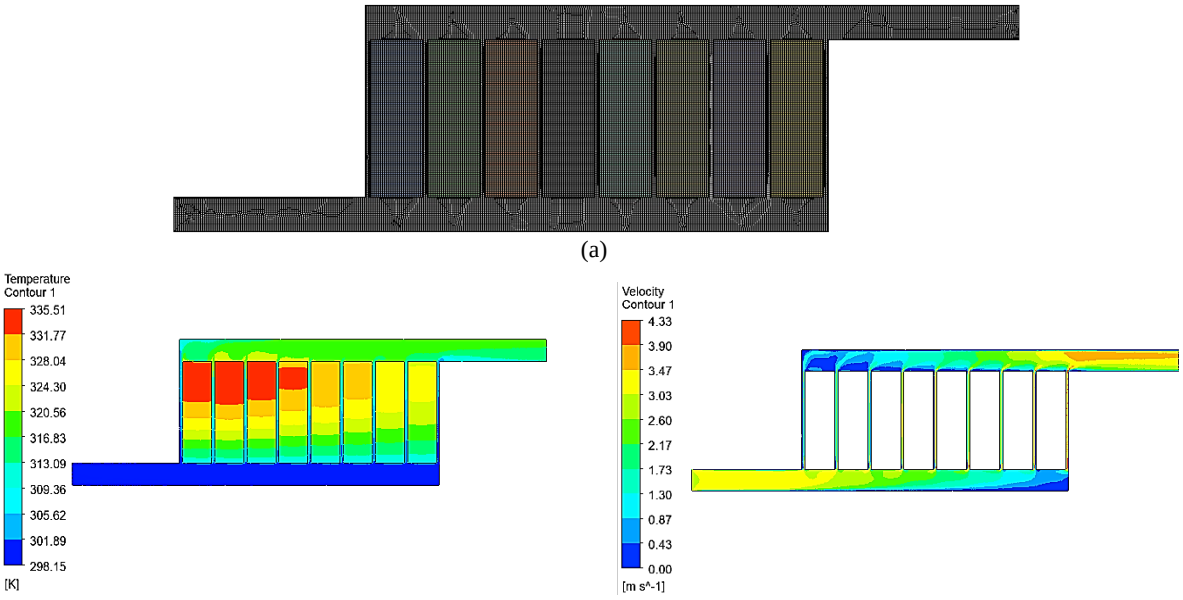

Figure 7. Z – Type BTMS; (a) Selected mesh, (b) Temperature contour, and (c) Velocity contour

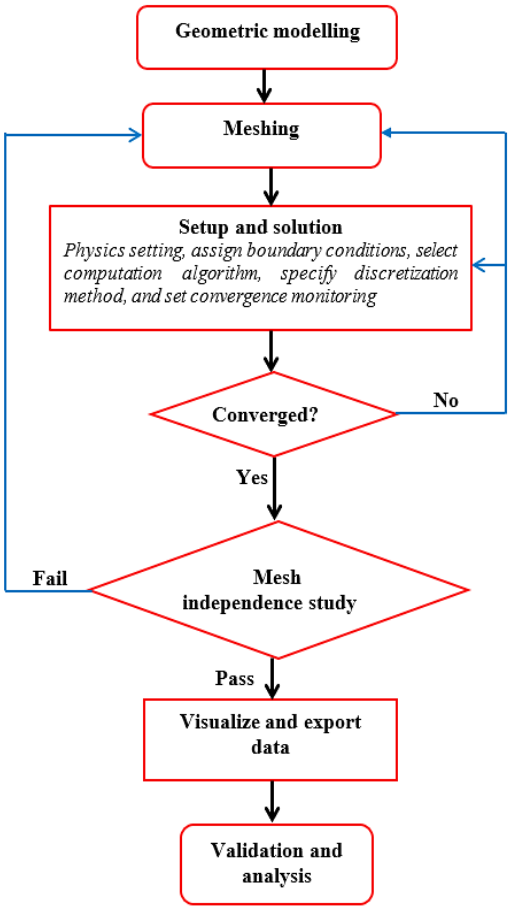

Figure 8. Flowchart of research methodology

3- Results and Discussion

The effects of several factors, including step angle, inlet cooling air velocity and temperature, and wall roughness, were investigated in this study. Results were obtained for original step-like BTMS and other BTMS with geometrical changes (Inclined steps). The T_{max} in a BTMS is widely reported as the primary parameter investigated. The recommended working temperature of lithium-ion battery desires that the temperature be maintained between 288 K and 318 K [3 – 5]. This temperature range could be influenced by ambient temperature, which varies by season and geographical location and, in most cases, also corresponds to the air-cooling temperature at the point of entry into the

BTMS. It is therefore essential to assess how variations in this temperature affect thermal performance, while targeting the previously reported acceptable working temperature range More so, while ensuring that the working temperature is targeted, ΔT_{max} of the multiple batteries working together must remain less than 5 ℃ (5 K) [3 – 5].

3-1- Effect of Step Slope Angles

The step-like plenum design has been studied to yield tangible thermal improvements [33, 37] due to the uniform air velocity it produces along the airflow path in the divergence plenum. The uniformity occurs due to flow obstruction by the vertical step height and the reduction of the airflow channel cross-sectional area from the 1st battery to the 8th battery. However, due to the ΔP, the steps increase the pressure drop between the inlet and outlet sections. To minimize the ΔP, consider redesigning the step height by adopting inclined steps, by changing the angle between the step height and the floor surface of the divergence plenum.

The performances of the inclined angles are presented in Figures 9 (a) and (b), showing temperature on the batteries and pressure drop in the systems, respectively. Furthermore, Figure 10 (a) shows the performance of T_{max} and ΔT_{max}, while Figure 10 (b) shows performance of T_{max} and ΔP. As reported in the previous studies [33, 37], step-like plenum significantly improved the temperature distribution on the batteries. By comparing the original Z-type BTMS with the step designs, a significant reduction of T_{max} was achieved. The original step-like design, yielded the best thermal performance, reducing the T_{max} by 4.42 K, while the other step designs with inclined angles 5°, 45° and 85° reduced the T_{max} by 3.18 K, 3.9 K, and 4.34 K, respectively. Despite all the inclined designs performing better than the Z-type design in reducing T_{max}, the original step-like design still yielded better performance with negligible variations. The variations of ΔP are illustrated in Figure 9 (b), with the Z-type design having the lowest value of 16.50 Pa, while the original step-like design has the highest value (undesirable) as 20.96 Pa. This implies that the inclined designs can be implemented where the reduction in ΔP is prioritized over the negligible variations in T_{max}, especially when the T_{max} falls within the recommended working temperature range of 288 K and 318 K [3-5]. From Figure 10 (a), the temperature performance of the designs shows a trend of reduced T_{max} with an increase in inclined angle. The temperature contour on the BTMSs is shown as Figures 11 (a) to (d), for angles of 5°, 45°, 85°and 90°, respectively.

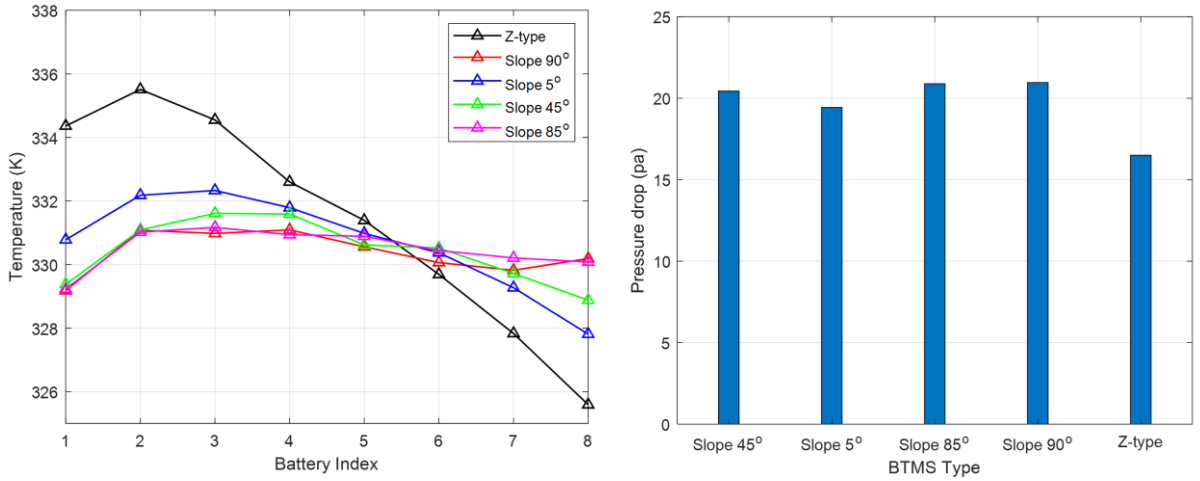

(a) (b)

Figure 9. (a) Temperature on battery, and (b) Pressure drop, at inlet air velocity of 3 m/s and air inlet temperature of 298.15 K

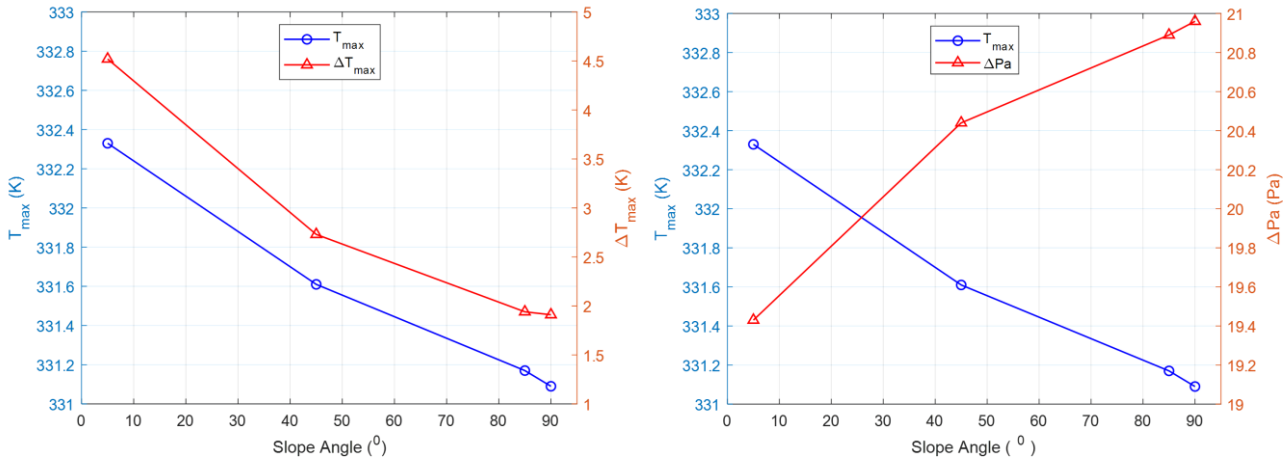

(a) (b)

Figure 10. Comparison of (a) T_{max} and ΔT_{max}, and (b) T_{max} and ΔP at inlet air velocity of 3 m/s and temperature 298.15K

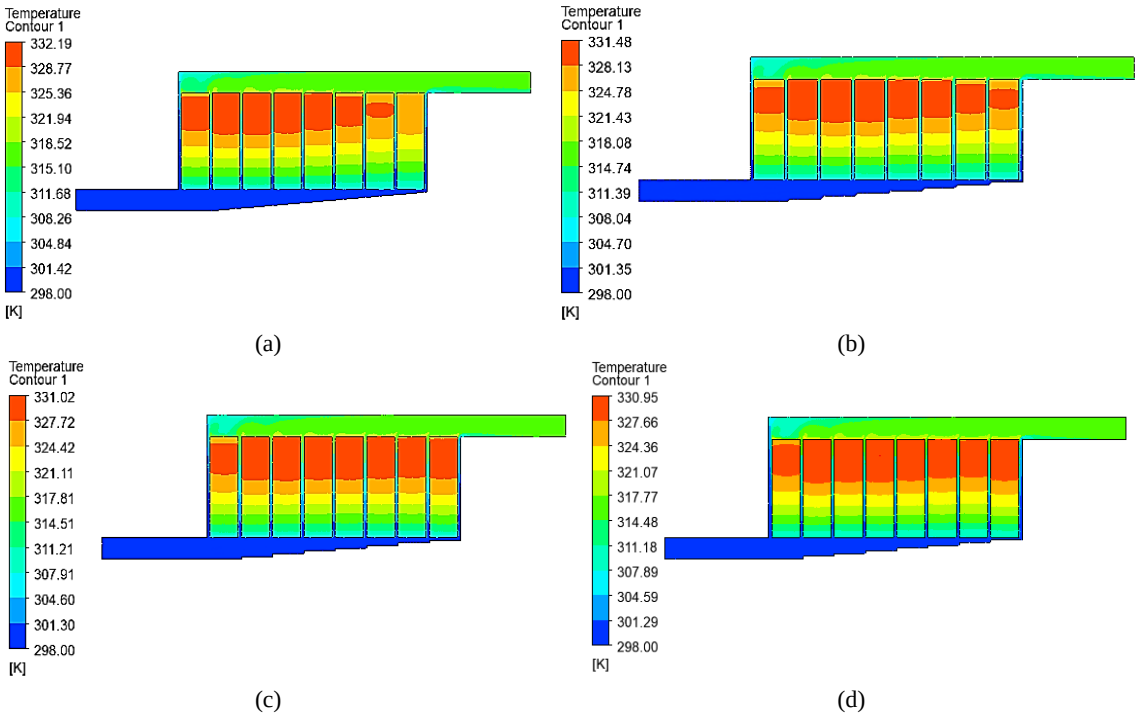

Figure 11. Temperature contours for inclined angles: (a) 5°, (b) 45°, (c) 85°, and (d) 90° (Original step-like design)

3-2- Effect of Inlet Velocity of Cooling Air

The inlet velocities of the cooling air initially studied are 3, 3.5, and 4 m/s, used to validate the numerical solution against experimental data. This study also compared the effects of air velocities 3, 5, and 7 m/s for the designs with original step-like design and inclined designs, air inlet temperature of 278K. The performance of the designs is shown in Figures 12 (a) to (c) for T_{max}, ΔT_{max} and ΔP, respectively. For the T_{max} values as shown in Figure 12 (a), as the inclined angle increases, the T_{max} decreases. The T_{max}value decreases with increasing air inlet velocity; however, a slight variation in the T_{max} performance was observed for the combined effect of increasing air inlet velocity and inclined angle. For instance, comparison between inclined angles 85° and 90°, reveals differences in their T_{max} are 0.09 K, 0.06 K, and 0.04 K, at air inlet velocities 3, 5, and 7 m/s. This implies that at higher air inlet temperatures, two inclined angle designs can produce T_{max} with negligible difference. From the T_{max} performance in Figure 12 (a), a design with a specific inclined angle can be employed when the value satisfies the recommended minimum $(288\ K)$ and maximum (318 K) allowable temperatures. The values of T_{max} shown in Figure 12 (a), falls within the range, with the highest, $T_{max} = 312.18\ K$ and lowest, $T_{min} = 296.38\ K$. The deduction from these performances indicate that for the range of air inlet velocities investigated, at an air inlet temperature of 278 K, the design with any of the inclined angles can be employed. In such case, the preferred design will be the design with the lowest ΔP.

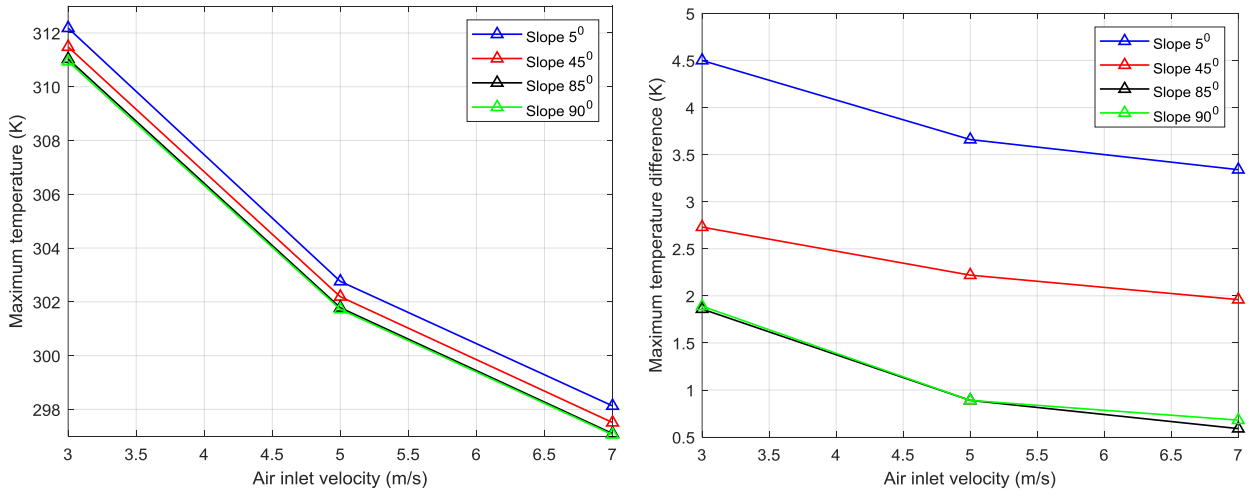

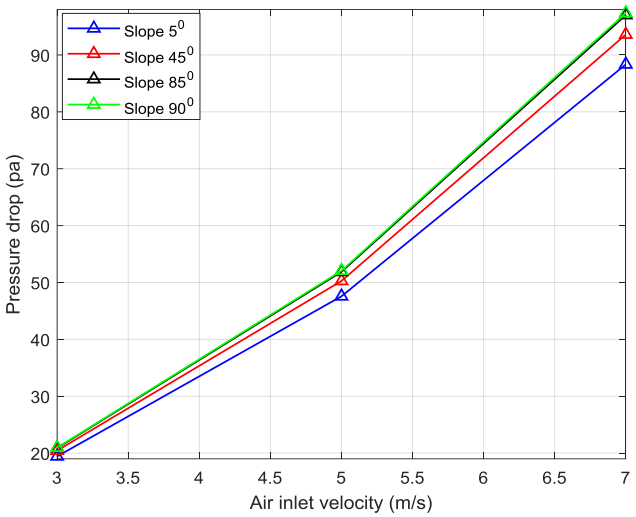

(c)

Figure 12. Comparison of (a) T_{max}, (b) ΔT_{max} and (c) ΔP at inlet air velocity of 3, 5, and 7m/s

The ΔT_{max} in the systems is also an essential parameter in the design of BTMSs. This parameter is recommended to be maintained below 5 K. From Figure 12 (b), it can be seen that ΔT_{max} decreases with an increase in air inlet velocity, while an increase in inclined angle results in a reduction in ΔT_{max}. Interestingly, the performance trend also shows variation when inclined angles 85° and 90° are compared. As shown in the figure, the differences between the ΔT_{max} values are 0.03 K, 0 K and 0.09 K at air inlet velocities 3 m/s, 5 m/s, and 7 m/s, respectively. This indicates that at 5 m/s, the two angles produced the same ΔT_{max}, while at 7 m/s, the ΔT_{max} values differ. A general deduction from the performance implies that higher inclined angle promotes thermal uniformity. When considering the recommended maximum allowable $\Delta T_{max} = 5\ K$, all the designs in Figure 12 (b) can be employed. The performance of the designs in terms of pressure drop, presented in Figure 12 (c), further establishes the change in the performance of the systems at high air inlet velocity. As shown in the figure, firstly, it can be seen that the pressure drop increases with an increase in air inlet velocity, and secondly, the difference between the pressure drop values of the inclined angles widens as air inlet velocity increases.

3-3- Effect of Inlet Temperature of Cooling Air

Figure 13 (a), shows the T_{max} of the designs in terms of inclined angles and the increase in air inlet temperature, for air inlet velocity 3 m/s. It is well known that the lowest inlet velocity will yield the highest T_{max} in the systems. However, it is also favourable due to the lowest pumping cost it will require. Hence, the lowest air inlet velocity was used for the comparison to determine the highest possible T_{max}, with an increase in air inlet temperature. Additionally, Figures 13 (b) and (c) present the ΔT_{max} performance with an increase in air inlet velocity. The performance of T_{max} with increasing air inlet temperature is presented in Figure 13 (a), clearly showing that the maximum system temperature increases with increasing in air inlet temperature. When considering the T_{max} from the performance in Figure 13 (a), all the inclined angles can be employed when air inlet temperature is $\leq$ 285 K, to satisfy the acceptable maximum allowable operating temperature of 318 K.

However, in a situation whereby higher air inlet velocity is adopted, the T_{max} values will reduce for all the cases and the systems can operate within the maximum allowable temperature of 318 K, air inlet temperature is $\geq$ 285 K, noted earlier. It should also be noted that increasing the air inlet temperature will consequently lead to an increase in pumping costs due to the higher pressure drop it causes Furthermore, due to the closeness and slight inconsistencies in the performance of designs with inclined angle 85° and 90°, the variation of ΔT_{max} was investigated for the two angles, when the air inlet velocities increase. Figure 13 (b) shows the performance for an inclined angle 85° and it was observed that at low air inlet velocity of 3 m/s and air inlet temperature of 278 K, the ΔT_{max} is lower than the air inlet temperatures of 298 and 318 K, whose values have an insignificant difference. However, for the inclined angle of 90° shown in Figure 13 (c), the difference between the ΔT_{max} values revealed inconsistencies for each of the air inlet velocities considered. The designs with inclined angle 85° and 90° also show satisfactory ΔT_{max} performance, because the ΔT_{max} values estimated were both less than 2 K, which is reasonably below the recommended maximum value of 5 K.

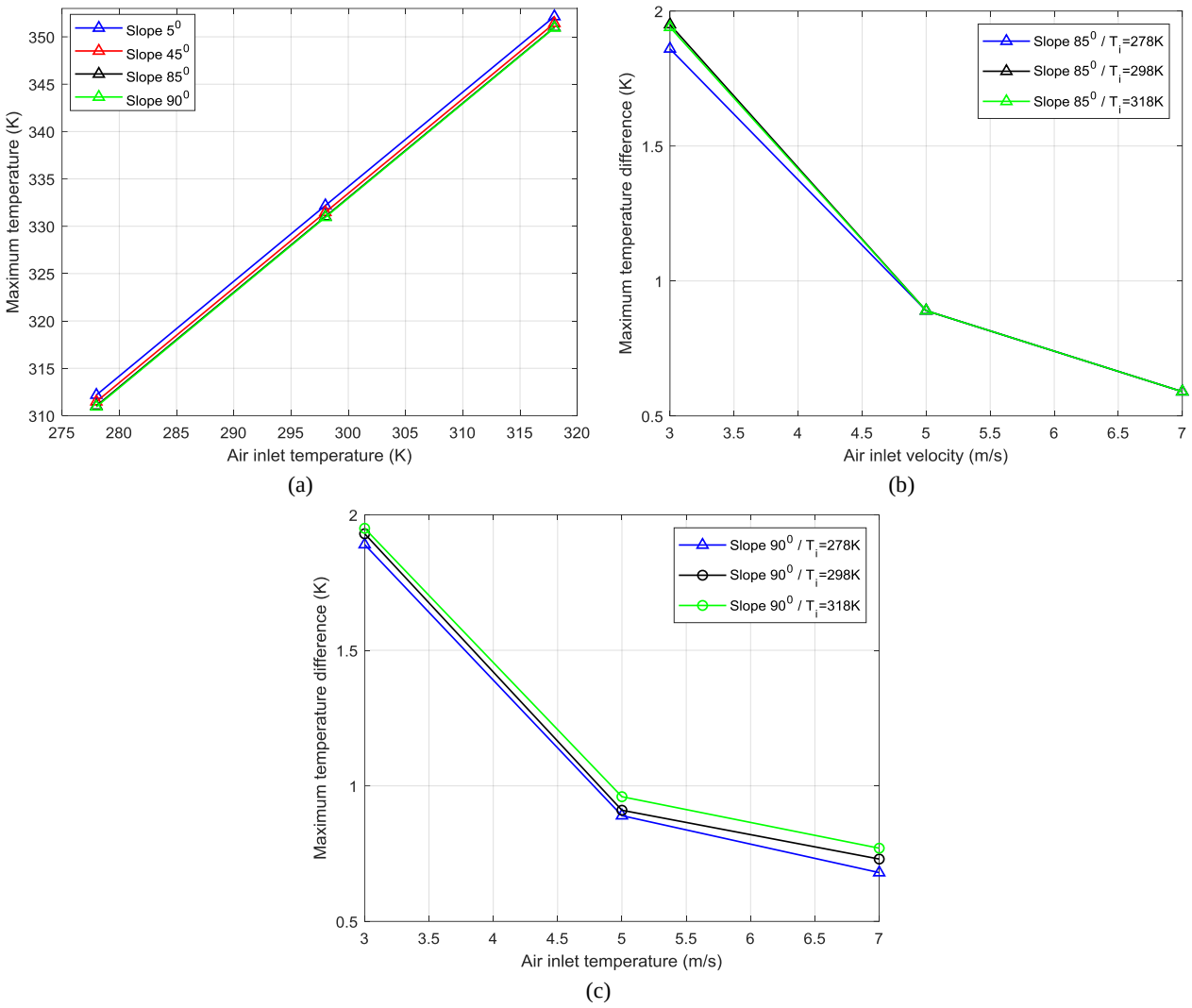

Figure 13. Comparison of (a) T_{max} and (b) ΔT_{max} at inlet air temperatures 278, 298, 318 K

3-4- Effect of Wall Roughness

Most designs of Z-type and other BTMS configurations focused on smooth surfaces, with components such as baffles, fins, and spoilers installed to alter airflow paths and enhance heat transfer performance. Without installing such components, the heat transfer and airflow behaviour in the BTMS can be influenced by adopting a rough surface as the BTMS's surrounding wall. In view of these, the wall roughness condition was assigned to the surrounding walls for the original Z-type design and inclined designs. Figure 14 shows the performance comparisons of T_{max} and ΔP relating to wall roughness for the Z-type BTMS.

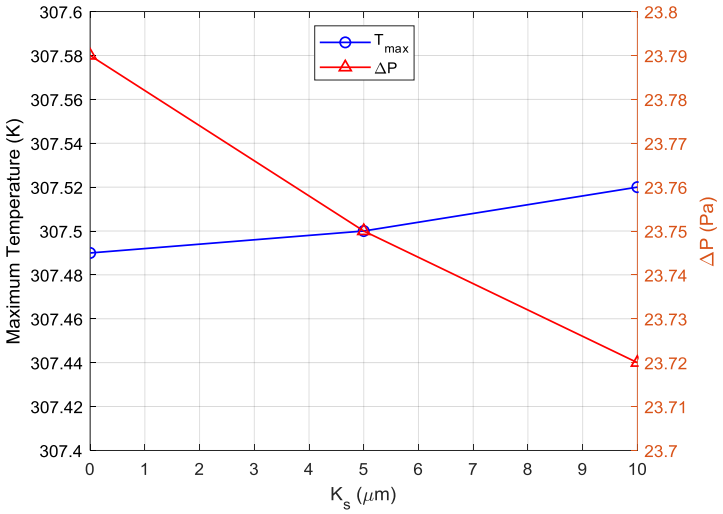

Figure 14. Effect of roughness height on T_{max} and ΔPon the original Z-Type BTMS

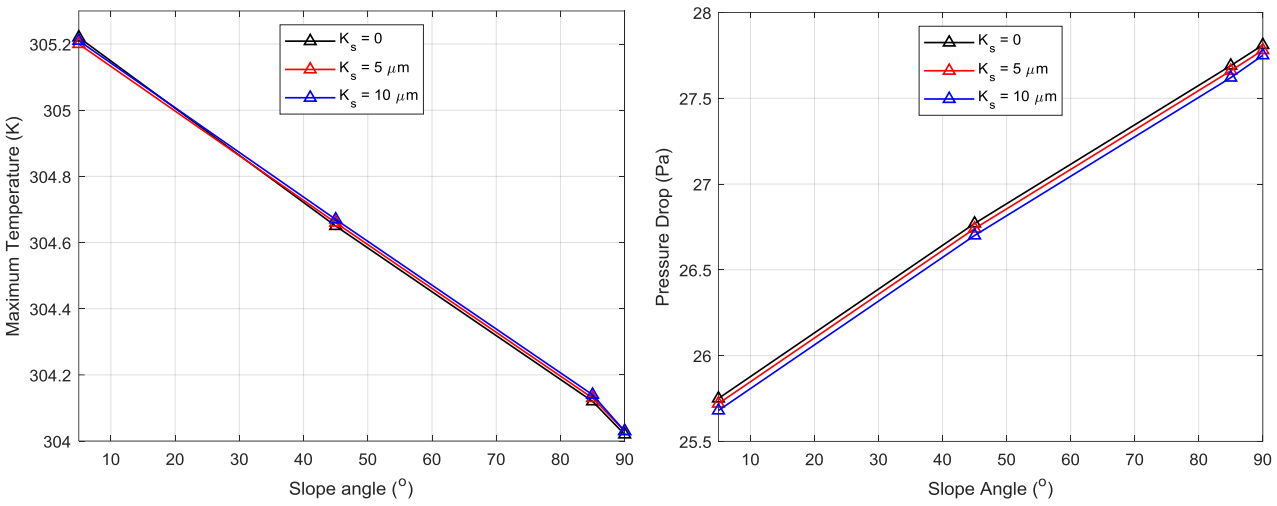

(a) (b)

Figure 15. Effects of roughness height and inclined angle on (a) T_{max} and (b) ΔP

Figure 14 shows the performance of the Z-type design without steps denoted as zero (0) for smooth surface, and rough surface having roughness heights 5 and 10 μm, while air inlet velocity of 3 m/s and air inlet temperature of 278 K were maintained. It can be seen that T_{max} increases when wall roughness is taken into account. Furthermore, by increasing the roughness height from 5 μm to 10 μm, an additional rise in T_{max} was observed. However, when considering ΔP, assigning wall roughness decreases ΔP and increasing roughness height also decreases ΔP. However, the increase and decrease in T_{max} and ΔP observed were very small. For instance, from 0 to 10 μm, T_{max} increased by 0.03 K (0.01 %) and ΔP increased by 0.07 Pa (0.29 %). The effect of roughness height and inclined angle on the performance of T_{max} and ΔP are presented in Figures 15(a) and (b), respectively. In the figure, the wall of the BTMS without roughness is denoted by '0', while the two other roughness heights are 5 and 10 μm. For the T_{max} performance, with smooth surface, the design with inclined angle '0' produced the poorest performance, while the designs with roughness heights of 5 and 10 μm produced the best performance. However, at inclined angles of 45° and 90°, the designs with smooth surfaces produced the best thermal performance. When considering pressure drop, an increase in inclined angle generally increases the pressure drop, while designs with smooth surfaces produced the maximum pressure drop values.

4- Conclusion

This study focused on the effects of step inclination, wall roughness, and air inlet velocity and temperature on step-like BTMS. The performance of the systems was evaluated in terms of T_{max}, ΔT_{max} and ΔP, using Computational Fluid Dynamics (CFD) method. Experimental data from the literature were used to validate the CFD method and the findings were evaluated. The results revealed that the original step-like design, produced the best thermal performance, which reduced the T_{max} by 4.42 K when compared with the original Z-Type deisgn. The other step designs with inclined angles 5°,45° and 85° reduced the T_{max} by 3.18 K, 3.9 K and 4.34 K, respectively. The Z-type design has the lowest ΔP value (16.50 Pa), while the original step-like design system produced the highest value (20.96 Pa). By comparing inclined angles 85° and 90°, the difference between their T_{max} are 0.09 K, 0.06 K and 0.04 K, at air inlet velocities 3 m/s, 5 m/s, and 7 m/s. For the T_{max}, a design with specific inclined angle can be employed when the value satisfies the recommended operating temperature of the batteries. When inclined angles 85° and 90° are compared at low air inlet temperature of 278 K, the values of T_{max} falls within the range recommended, with the highest, $T_{max} = 312.18\ K$ and lowest, $T_{min} = 296.38\ K$.

Additionally, for the effect of air inlet velocity ΔT_{max} was observed to be decreasing with increase in air inlet velocity, while an increase in inclined angle results to reduction in ΔT_{max}. The differences between the ΔT_{max} values are 0.03 K, 0 K and 0.09 K at air inlet velocities 3 m/s, 5 m/s, and 7 m/s, respectively. It was observed that T_{max} is influenced when wall roughness is considered. Furthermore, by increasing the roughness height from 5 μm to 10 μm, an additional increase in T_{max} was observed. However, when considering ΔP, assigning wall roughness decreases ΔP, while an increase in the roughness height decreased ΔP. However, the increase and decrease in T_{max} and ΔP observed were minimal. For instance, from 0 to 10 μm, T_{max} increased by 0.03 K (0.01 %) and ΔP increased by 0.07 Pa (0.29 %). The study, therefore, concludes that the outcome of the investigation will guide future studies aimed at exploring the step-like design across different applications and working conditions.

5- Nomenclature

Acronym	
CFD	Computational fluid dynamics
EV	Electric vehicles
UAV	Unmanned aerial vehicle
PCM	Phase change material
2D	Two dimensional
3D	Three dimensional
BTMS	Battery thermal management system
CC	Cooling channel
DP	Divergence plenum
CP	Convergence plenum
QCNN	Quantile convolutional neural network
ANN	Artificial neural network
ML	Machine learning
AC	Air cooling
PCMC	Phase change material cooling
NECC	Nano-enhanced channel cooling
HPC	Heat pipe cooling
LC	Liquid cooling
HC	Hybrid cooling
FELHP	Flat evaporator loop heat pipe
GA	Gravitational acceleration
VHTP	Variable heat transfer path

Symbols		Unit
C	Convergence	
D	Divergence	
N	Number	
H	Height	mm
L	Length	mm
P	Pressure	Pa
A	Cross-sectional area at inlet and outlet sections	m^2
$\dot{V}$	Volume flow rate	m^3/s
v	Air velocity at the inlet	m/s
u	Velocity vector	m/s
x	x-coordinate	m
W	Width of manifold	mm
Re	Reynolds number	-
T	Temperature	K
t	Time	s
Q	Rate of heat generation	W
k	Thermal conductivity	W/mK
c	Specific heat capacity	J/kgK
D_h	Hydraulic diameter	mm
K_s	Surface roughness height	mm
C_s	Surface roughness constant	-
G_k *and* G_b	Turbulence kinetic energy generation due to the average velocity gradients and buoyancy effects, respectively	
Y_M	Contribution of fluctuating dilatation in compressible turbulence to the overall dissipation rate	
$C_{1\varepsilon}, C_{2\varepsilon}, C_{3\varepsilon}$	Model constants	
S_k *and* S_ϵ	Source terms	

Greek letters		
θl	Inclination angle	°
ρ	Density	kg/m^3
μ	Dynamic viscosity	kg/ms
σ_k, σ_ϵ	k and ε turbulent Prandtl numbers	
Δ	Change/Difference	
∇	Gradient operator	
Subscripts		
B	Battery	
s	Step	
in	Inlet	
out	Outlet	
max	Maximum	
min	Minimum	
avg	Average	
i	ith component	
t	Turbulent	
l	Length	
c	Cooling section	
p	Plenum	

6- Declarations

6-1- Author Contributions

Conceptualization, O.O.; methodology, O.O., E.I., M.L., M.H., and M.D.; software, O.O., E.I., M.L., M.H., and M.D.; validation, O.O., E.I., M.L., M.H., and M.D.; formal analysis, O.O., E.I., M.L., M.H., and M.D.; investigation, O.O., E.I., M.L., M.H., and M.D.; resources, O.O.; data curation, O.O., E.I., M.L., M.H., and M.D.; writing—original draft preparation, O.O., E.I., M.L., M.H., and M.D.; writing—review and editing, O.O., E.I., M.L., M.H., and M.D.; visualization, O.O., E.I., M.L., M.H., and M.D.; project administration, O.O.; funding acquisition, O.O. All authors have read and agreed to the published version of the manuscript.

6-2- Data Availability Statement

The data presented in this study are available on request from the corresponding author.

6-3- Funding

The authors received no financial support for the research, authorship, and/or publication of this article.

6-4- Institutional Review Board Statement

Not applicable.

6-5- Informed Consent Statement

Not applicable.

6-6- Conflicts of Interest

The authors declare that there is no conflict of interest regarding the publication of this manuscript. In addition, the ethical issues, including plagiarism, informed consent, misconduct, data fabrication and/or falsification, double publication and/or submission, and redundancies have been completely observed by the authors.

7- References

[1] Babu Sanker, S., & Baby, R. (2022). Phase change material based thermal management of lithium-ion batteries: A review on thermal performance of various thermal conductivity enhancers. Journal of Energy Storage, 50, 104606. doi:10.1016/j.est.2022.104606.

[2] Yang, Y., Okonkwo, E. G., Huang, G., Xu, S., Sun, W., & He, Y. (2021). On the sustainability of lithium-ion battery industry – A review and perspective. Energy Storage Materials, 36, 186–212. doi:10.1016/j.ensm.2020.12.019.

[3] Saw, L. H., Ye, Y., Tay, A. A. O., Chong, W. T., Kuan, S. H., & Yew, M. C. (2016). Computational fluid dynamic and thermal analysis of Lithium-ion battery pack with air cooling. Applied Energy, 177, 783–792. doi:10.1016/j.apenergy.2016.05.122.

[4] Dan, D., Yao, C., Zhang, Y., Zhang, H., Zeng, Z., & Xu, X. (2019). Dynamic thermal behavior of micro heat pipe array-air cooling battery thermal management system based on thermal network model. Applied Thermal Engineering, 162, 114183. doi:10.1016/j.applthermaleng.2019.114183.

[5] Zhong, G., Zhang, G., Yang, X., Li, X., Wang, Z., Yang, C., Yang, C., & Gao, G. (2017). Researches of composite phase change material cooling/resistance wire preheating coupling system of a designed 18650-type battery module. Applied Thermal Engineering, 127, 176–183. doi:10.1016/j.applthermaleng.2017.08.022.

[6] Akinlabi, A. A. H., & Solyali, D. (2020). Configuration, design, and optimization of air-cooled battery thermal management system for electric vehicles: A review. Renewable and Sustainable Energy Reviews, 125, 109815. doi:10.1016/j.rser.2020.109815.

[7] Behi, H., Karimi, D., Behi, M., Ghanbarpour, M., Jaguemont, J., Sokkeh, M. A., Gandoman, F. H., Berecibar, M., & Van Mierlo, J. (2020). A new concept of thermal management system in Li-ion battery using air cooling and heat pipe for electric vehicles. Applied Thermal Engineering, 174, 115280. doi:10.1016/j.applthermaleng.2020.115280.

[8] Zhang, F., Lin, A., Wang, P., & Liu, P. (2021). Optimization design of a parallel air-cooled battery thermal management system with spoilers. Applied Thermal Engineering, 182, 116062. doi:10.1016/j.applthermaleng.2020.116062.

[9] Wang, M., Teng, S., Xi, H., & Li, Y. (2021). Cooling performance optimization of air-cooled battery thermal management system. Applied Thermal Engineering, 195, 117242. doi:10.1016/j.applthermaleng.2021.117242.

[10] Alzwayi, A., & Paul, M. C. (2024). Heat transfer enhancement of a lithium-ion battery cell using vertical and spiral cooling fins. Thermal Science and Engineering Progress, 47, 102304. doi:10.1016/j.tsep.2023.102304.

[11] Liang, J., Gan, Y., & Li, Y. (2018). Investigation on the thermal performance of a battery thermal management system using heat pipe under different ambient temperatures. Energy Conversion and Management, 155, 1–9. doi:10.1016/j.enconman.2017.10.063.

[12] Liang, Z., Wang, R., Malt, A. H., Souri, M., Esfahani, M. N., & Jabbari, M. (2021). Systematic evaluation of a flat-heat-pipe-based thermal management: Cell-to-cell variations and battery ageing. Applied Thermal Engineering, 192(5), 116934. doi:10.1016/j.applthermaleng.2021.116934.

[13] Panchal, S., Khasow, R., Dincer, I., Agelin-Chaab, M., Fraser, R., & Fowler, M. (2017). Thermal design and simulation of mini-channel cold plate for water cooled large sized prismatic lithium-ion battery. Applied Thermal Engineering, 122, 80–90. doi:10.1016/j.applthermaleng.2017.05.010.

[14] Rao, Z., Qian, Z., Kuang, Y., & Li, Y. (2017). Thermal performance of liquid cooling based thermal management system for cylindrical lithium-ion battery module with variable contact surface. Applied Thermal Engineering, 123, 1514–1522. doi:10.1016/j.applthermaleng.2017.06.059.

[15] Fathabadi, H. (2014). High thermal performance lithium-ion battery pack including hybrid active-passive thermal management system for using in hybrid/electric vehicles. Energy, 70, 529–538. doi:10.1016/j.energy.2014.04.046.

[16] Rao, Z., Wang, Q., & Huang, C. (2016). Investigation of the thermal performance of phase change material/mini-channel coupled battery thermal management system. Applied Energy, 164, 659–669. doi:10.1016/j.apenergy.2015.12.021.

[17] Samimi, F., Babapoor, A., Azizi, M., & Karimi, G. (2016). Thermal management analysis of a Li-ion battery cell using phase change material loaded with carbon fibers. Energy, 96, 355–371. doi:10.1016/j.energy.2015.12.064.

[18] Qin, P., Liao, M., Mei, W., Sun, J., & Wang, Q. (2021). The experimental and numerical investigation on a hybrid battery thermal management system based on forced-air convection and internal finned structure. Applied Thermal Engineering, 195, 117212. doi:10.1016/j.applthermaleng.2021.117212.

[19] Sharma, D. K., Agarwal, P., & Prabhakar, A. (2023). Effect of fin design and continuous cycling on thermal performance of PCM-HP hybrid BTMS for high ambient temperature applications. Journal of Energy Storage, 74(Part B), 109360. doi:10.1016/j.est.2023.109360.

[20] Mashayekhi, M., Houshfar, E., & Ashjaee, M. (2020). Development of hybrid cooling method with PCM and Al2O3 nanofluid in aluminium minichannels using heat source model of Li-ion batteries. Applied Thermal Engineering, 178, 115543. doi:10.1016/j.applthermaleng.2020.115543.

[21] Xie, N., Zhang, Y., Liu, X., Luo, R., Liu, Y., & Ma, C. (2023). Thermal performance and structural optimization of a hybrid thermal management system based on MHPA/PCM/liquid cooling for lithium-ion battery. Applied Thermal Engineering, 235, 121341. doi:10.1016/j.applthermaleng.2023.121341.

[22] Chen, K., Wang, S., Song, M., & Chen, L. (2017). Configuration optimization of battery pack in parallel air-cooled battery thermal management system using an optimization strategy. Applied Thermal Engineering, 123, 177–186. doi:10.1016/j.applthermaleng.2017.05.060.

[23] Chen, K., Wu, W., Yuan, F., Chen, L., & Wang, S. (2019). Cooling efficiency improvement of air-cooled battery thermal management system through designing the flow pattern. Energy, 167, 781–790. doi:10.1016/j.energy.2018.11.011.

[24] Chen, K., Song, M., Wei, W., & Wang, S. (2019). Design of the structure of battery pack in parallel air-cooled battery thermal management system for cooling efficiency improvement. International Journal of Heat and Mass Transfer, 132, 309–321. doi:10.1016/j.ijheatmasstransfer.2018.12.024.

[25] Chen, K., Chen, Y., Li, Z., Yuan, F., & Wang, S. (2018). Design of the cell spacings of battery pack in parallel air-cooled battery thermal management system. International Journal of Heat and Mass Transfer, 127, 393–401. doi:10.1016/j.ijheatmasstransfer.2018.06.131.

[26] Jiaqiang, E., Yue, M., Chen, J., Zhu, H., Deng, Y., Zhu, Y., Zhang, F., Wen, M., Zhang, B., & Kang, S. (2018). Effects of the different air cooling strategies on cooling performance of a lithium-ion battery module with baffle. Applied Thermal Engineering, 144, 231–241. doi:10.1016/j.applthermaleng.2018.08.064.

[27] Wang, N., Li, C., Li, W., Huang, M., & Qi, D. (2021). Effect analysis on performance enhancement of a novel air cooling battery thermal management system with spoilers. Applied Thermal Engineering, 192, 116932. doi:10.1016/j.applthermaleng.2021.116932.

[28] Oyewola, O. M., Ismail, O. S., & Awonusi, A. A. (2022). Examination of Channel Angles Influence on the Cooling Performance of Air-cooled Thermal Management System of Li-Ion Battery. International Review of Mechanical Engineering, 16(4), 172–179. doi:10.15866/ireme.v16i4.22239.

[29] Sun, H., & Dixon, R. (2014). Development of cooling strategy for an air cooled lithium-ion battery pack. Journal of Power Sources, 272, 404–414. doi:10.1016/j.jpowsour.2014.08.107.

[30] Chen, J., Zhao, X., Wang, B., Zhang, C., & Xuan, D. (2021). Multiobjective optimization of air-cooled battery thermal management system based on heat dissipation model. Ionics, 27(3), 1307–1322. doi:10.1007/s11581-020-03853-6.

[31] Chen, K., Hou, J., Wu, X., Chen, Y., Song, M., & Wang, S. (2021). Design of flow pattern in air-cooled battery thermal management system. International Journal of Energy Research, 45(6), 9541–9554. doi:10.1002/er.6480.

[32] Chen, K., Song, M., Wei, W., & Wang, S. (2018). Structure optimization of parallel air-cooled battery thermal management system with U-type flow for cooling efficiency improvement. Energy, 145, 603–613. doi:10.1016/j.energy.2017.12.110.

[33] Oyewola, O. M., Awonusi, A. A., & Ismail, O. S. (2023). Design optimization of Air-Cooled Li-ion battery thermal management system with Step-like divergence plenum for electric vehicles. Alexandria Engineering Journal, 71, 631–644. doi:10.1016/j.aej.2023.03.089.

[34] Chen, K., Wang, S., Song, M., & Chen, L. (2017). Structure optimization of parallel air-cooled battery thermal management system. International Journal of Heat and Mass Transfer, 111, 943–952. doi:10.1016/j.ijheatmasstransfer.2017.04.026.

[35] Yu, K., Yang, X., Cheng, Y., & Li, C. (2014). Thermal analysis and two-directional air flow thermal management for lithium-ion battery pack. Journal of Power Sources, 270, 193–200. doi:10.1016/j.jpowsour.2014.07.086.

[36] Wang, M., Hung, T. C., & Xi, H. (2021). Numerical study on performance enhancement of the air-cooled battery thermal management system by adding parallel plates. Energies, 14(11), 3096. doi:10.3390/en14113096.

[37] Oyewola, O. M., & Idowu, E. T. (2024). Effects of step-like plenum, flow pattern and inlet flow regime on thermal management system. Applied Thermal Engineering, 243, 122637. doi:10.1016/j.applthermaleng.2024.122637.

[38] Li, N., Liu, X., Yu, B., Li, L., Xu, J., & Tan, Q. (2021). Study on the environmental adaptability of lithium-ion battery powered UAV under extreme temperature conditions. Energy, 219, 119481. doi:10.1016/j.energy.2020.119481.

[39] Wei, W., Luo, Z., Qiao, S., Zhai, J., & Lei, Z. (2024). Analysis and design of module-level liquid cooling system for rectangular Li-ion batteries. International Journal of Heat and Mass Transfer, 225, 125435. doi:10.1016/j.ijheatmasstransfer.2024.125435.

[40] Verma, S. P., & Saraswati, S. (2024). Comprehensive thermal performance analysis of an air-cooled staggered configured Li-ion battery pack- A numerical and experimental approach. Journal of Energy Storage, 89. doi:10.1016/j.est.2024.111792.

[41] Tran, M. K., Panchal, S., Chauhan, V., Brahmbhatt, N., Mevawalla, A., Fraser, R., & Fowler, M. (2022). Python-based scikit-learn machine learning models for thermal and electrical performance prediction of high-capacity lithium-ion battery. International Journal of Energy Research, 46(2), 786–794. doi:10.1002/er.7202.

[42] Billert, A. M., Erschen, S., Frey, M., & Gauterin, F. (2022). Predictive battery thermal management using quantile convolutional neural networks. Transportation Engineering, 10, 100150. doi:10.1016/j.treng.2022.100150.

[43] Najafi Khaboshan, H., Jaliliantabar, F., Abdullah, A. A., Panchal, S., & Azarinia, A. (2024). Parametric investigation of battery thermal management system with phase change material, metal foam, and fins; utilizing CFD and ANN models. Applied Thermal Engineering, 247(15), 123080. doi:10.1016/j.applthermaleng.2024.123080.

[44] Oyewola, O. M., & Idowu, E. T. (2024). Wave and straight plenum effects on thermal management system performance. International Journal of Thermofluids, 22, 100678. doi:10.1016/j.ijft.2024.100678.

[45] Zare, P., Perera, N., Lahr, J., & Hasan, R. (2024). A novel thermal management system for cylindrical lithium-ion batteries using internal-external fin-enhanced phase change material. Applied Thermal Engineering, 238, 121985. doi:10.1016/j.applthermaleng.2023.121985.

[46] Wu, C., Qiu, C., Yuan, X., Yuan, N., Zhang, B., Li, Y., Qin, L., & Shi, H. (2024). Numerical study and optimization of battery thermal management systems (BTMS) Based on Fin-Phase change material (PCM) in variable gravity environments. Applied Thermal Engineering, 244, 122777. doi:10.1016/j.applthermaleng.2024.122777.

[47] Suo, Y., Tang, C., Jia, Q., & Zhao, W. (2024). Influence of PCM configuration and optimization of PCM proportion on the thermal management of a prismatic battery with a combined PCM and air-cooling structure. Journal of Energy Storage, 80, 110340. doi:10.1016/j.est.2023.110340.

[48] Bernagozzi, M., Georgoulas, A., Miché, N., & Marengo, M. (2024). Experimental analysis of the influence of ambient temperature for a Loop Heat Pipe based Battery Thermal Management System. Experimental and Computational Multiphase Flow, 6(3), 242–252. doi:10.1007/s42757-023-0185-5.

[49] Wu, C., Ni, J., Shi, X., & Huang, R. (2024). A new design of cooling plate for liquid-cooled battery thermal management system with variable heat transfer path. Applied Thermal Engineering, 239, 122107. doi:10.1016/j.applthermaleng.2023.122107.

[50] Wu, C., Yuan, X., Kong, B., Zou, Y., & Shi, H. (2024). Innovative liquid cooling channel enhanced battery thermal management (BTM) structure based on stepwise optimization method. Journal of Energy Storage, 81, 110485. doi:10.1016/j.est.2024.110485.

[51] Dilbaz, F., Selimefendigil, F., & Öztop, H. F. (2024). Comparisons of different cooling systems for thermal management of lithium-ion battery packs: Phase change material, nano-enhanced channel cooling and hybrid method. Journal of Energy Storage, 90, 111865. doi:10.1016/j.est.2024.111865.

[52] Lu, D., Cui, N., Zhou, J., & Li, C. (2024). Hybrid cooling system with phase change material and liquid microchannels to prevent thermal runaway propagation within lithium-ion battery packs. Applied Thermal Engineering, 247, 123118. doi:10.1016/j.applthermaleng.2024.123118.

[53] Rahjoo, M., Rojas, E., Goracci, G., & Dolado, J. S. (2024). Exploring the role of surface roughness in concrete-based thermal energy storage systems: A computational study. Journal of Energy Storage, 88, 111515. doi:10.1016/j.est.2024.111515.

[54] Cebeci, T. (2004). Conservation Equations for Compressible Turbulent Flows. Analysis of Turbulent Flows, 31–48. doi:10.1016/b978-008044350-8/50002-6.

[55] Kadivar, M., Tormey, D., & McGranaghan, G. (2021). A review on turbulent flow over rough surfaces: Fundamentals and theories. International Journal of Thermofluids, 10, 100077. doi:10.1016/j.ijft.2021.100077.